ATM #1099
1 May 1972

PRELIMINARY TEST EVALUATION ON LSPE HAZARD ANALYSIS

Prepared by G. B. Min
G. B. Min, Ph. D.

Approved by J. Zimmer
J. Zimmer

Approved by L. R. Lewis
L. R. Lewis, Manager
Lunar Seismic Profiling Experiment

TABLE OF CONTENTS

ABSTRACT

The Lunar Seismic Profiling Experiment (LSPE) includes a chain of eight explosive packages which are to be detonated on the lunar surface. The purpose of this report is to evaluate the data collected from a one-eighth pound charge detonated under a dome at a field test site. From these data the chance of hazard to the ALSEP Electronics Central Station (ECS) and to the orbiting Command Service Module (CSM) is assessed, preliminarily through extrapolation. The results show (1) that the chance of the ECS being impacted is .014047 with the major contribution being from lunar debris (.011728), and (2) that the chance of hazard to the CSM is 7.04×10^{-9}.

Two suggestions were generated from the observation of the test: align either of the package's diagonal lines toward the ECS to take advantage of minimum projectiles flying out in that direction, and deploy the packages so that any lunar surface protuberances lie between the ECS and the package. The chance of hazard to the ECS can be reduced greatly.

LIST OF FIGURES

I. INTRODUCTION

Eight explosive packages will be deployed and detonated on the lunar surface for the Lunar Seismic Profiling Experiment (LSPE) during the Apollo 17 mission. Due to the low gravitational field and the high vacuum lunar environment, the trajectories of fragments and debris greatly increase in altitude and range, thus possessing the potential hazard to the ALSEP Central Station and to the orbiting Command Service Module. Therefore, fragmentation and cratering profiles due to detonation must be accomplished to provide the data for the hazard analysis.

In order to provide experimental data to compare with the previous theoretical results presented in Bendix ATM 1079 report (1), one one-eighth pound charge, covered by a hemispherical dome with a 76-inch inside diameter, was detonated during prototype model field tests of the LSPE. Designed to trap debris and fragments, the dome has a four-inch polyurethane foam interior bonded to a two-tenths inch glass fiber exterior. By using the empirical correlation formula derived from the calibration test, the depth of penetration is correlated with mass, size and the observing geometry of the entrapment, to predict with some accuracy the velocity upon impact.

Due to the lack of one-fourth pound charge test data, the extrapolation to include all charges presented a problem in calculating velocity, distribution pattern, and probability. In order to compensate this deficiency the data collected by the SRI(2) Report on the Active Seismic Experiment is adapted. This report furnishes the velocity of different sized fragments from the detonation of a one-pound charge.

II. TEST SET-UP AND RECOVERY OF THE SPECIMENS

The deployed dome configuration is shown in Figure 1. The reference coordinates are based on the line which connects the Safe Arm Slide observation window and the antenna opening. The location of the off-center antenna opening allows the explosive charge to sit at the center of the hemisphere. This provides a good experimental correlation with the mathematical model using the blast center as an origin.

The pads supporting the dome were not allowed to lie over the ditch. Each pad was piled up with three sandbags to prevent upward movement due to the blast.

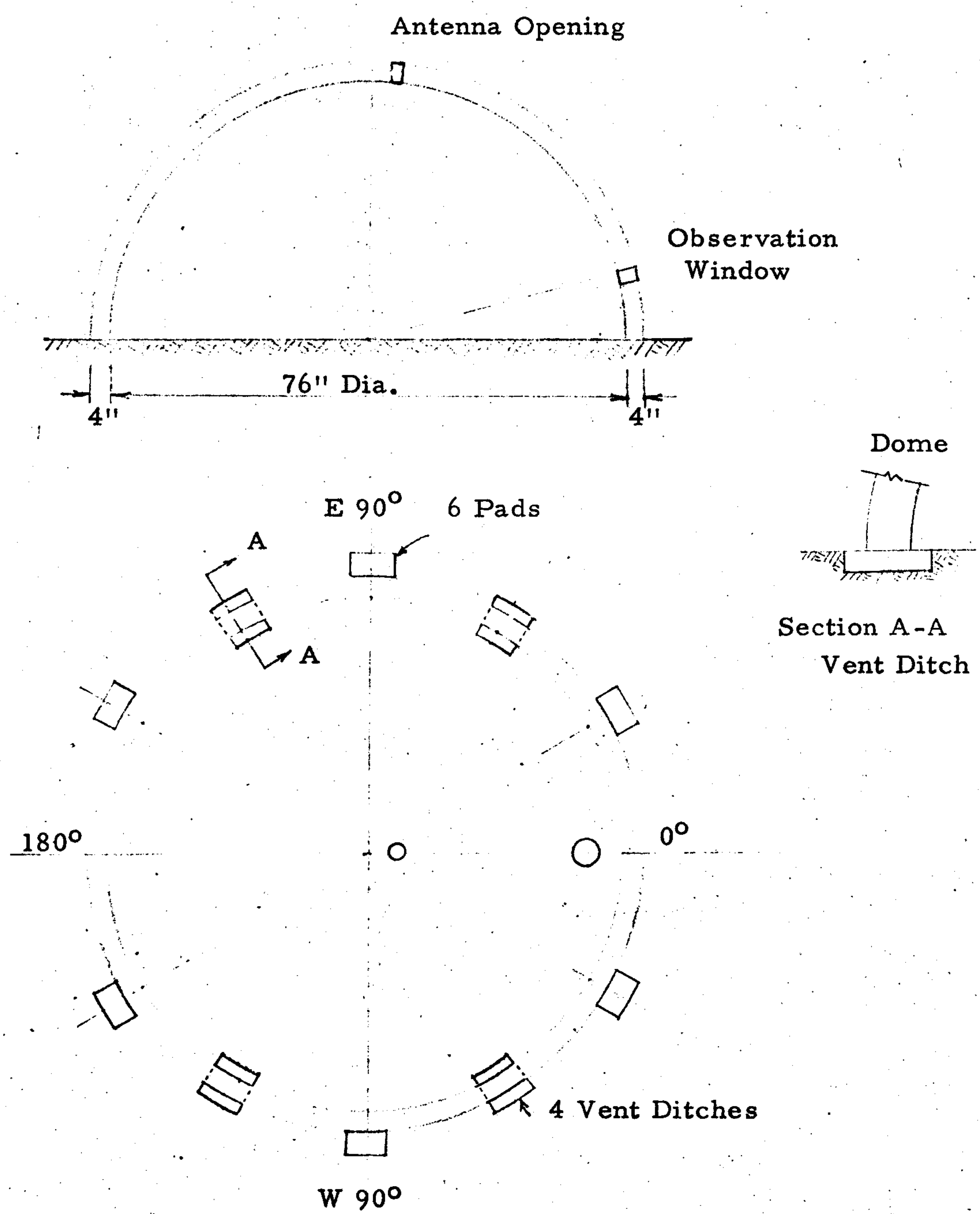

FIGURE 1: DOME ARRANGEMENT

The dome, being large in size and heavy in weight, required maximum field effort for the gathering of data after the blast. Inspection, locating points of penetration, cutting the dome, X-ray photography and recovering the fragments were all performed at the site. The X-ray photograph proved to be a very effective tool in recovering the embedded fragments which were not detectable by visual inspection. Some typical X-ray photographs which reveal the penetration pattern are presented in Figures 2, 3 and 4. A total of 118 fragments weighing 2.276 pounds were recovered from a package weight of 2.563 pounds (88.8% weight recovery). The unrecovered weight accounted for an additional 51 penetration points.

There were 85 visible, soil debris, penetration points. Most of these soil particles were crushed completely and were difficult to recover. The remainder of the soil debris (other than that recovered from the penetration points) consisted of fine soil particles which were spread over the impact area in decreasing intensity toward increasing flight angle as shown in Figure 5.

In addition to those fragments trapped in the dome, there were some pieces of fragment that dropped back to the ground as shown in Figure 6. The scattered foam pieces (also in Figure 6) did not originate from the explosive package but rather from the heating device.

There were three spalling spots on the surface of the dome as shown in Figure 7. This pattern came from a cluster impact with larger-sized fragments and from the material weakness due to the antenna opening in the vicinity.

III. PENETRATION AND DISTRIBUTION PATTERN

The distribution patterns of fragments and soil debris are described in Figure 8. The impacted areas were not uniformly distributed as had been expected; rather it is very significant that the concentration of impact occurred normal to the mid-point of the four experiment edges, each edge forming a normal distribution center. In order to visualize this pattern, all the fragment-penetrated locations were regenerated and plotted in Figure 9. This information provides a base for reconstructing two figures: Figure 10 for relative frequency of fragment distribution versus horizontal angle, and Figure 11 for relative frequency of fragment distribution versus initial flight angle. Figure 10 shows that a low impact frequency occurs along the outward direction of the four corners. This information is significant in reducing the possible hazard to the Central Station. In Figure 11 the number of high flight angles decreases rapidly, but the fragment weight increases toward the increase of flight angle. This pattern is attributed to the configuration of the explosive package.

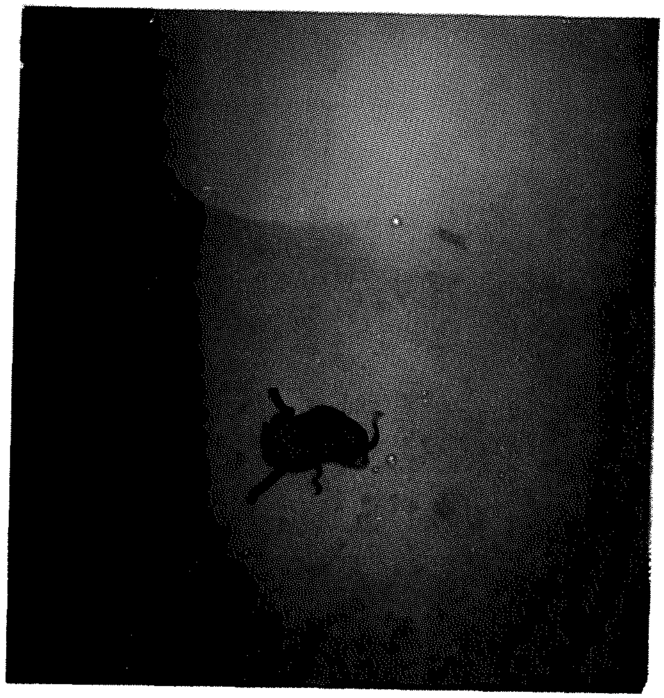

(a) Top X-Ray View

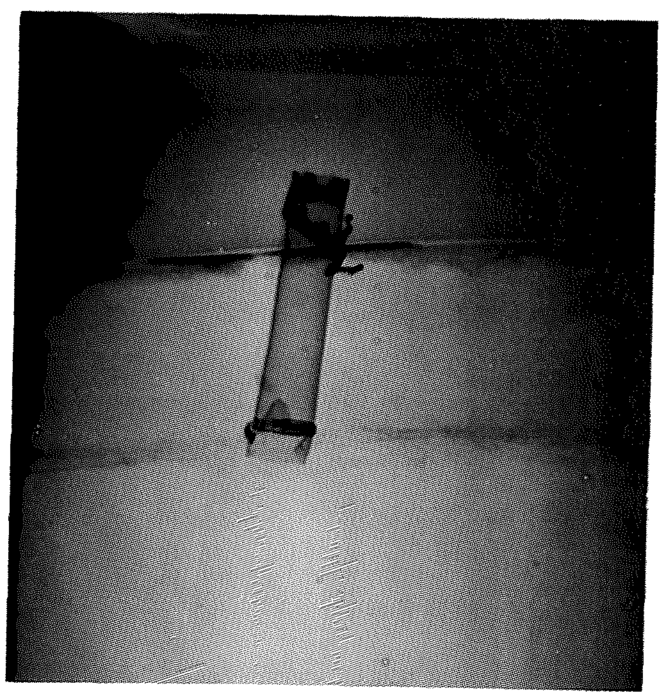

(b) Section View

FIGURE 2: Penetration of Antenna Tube into Dome Material

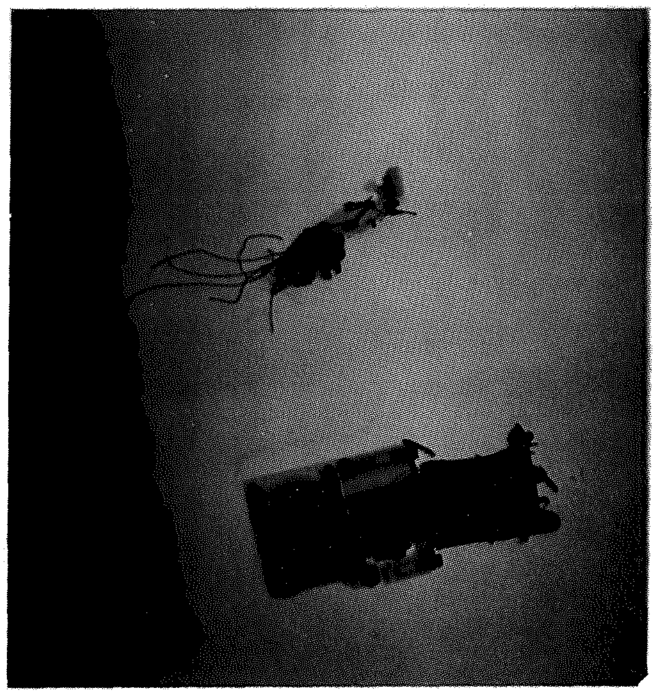

(a) Top X-Ray View

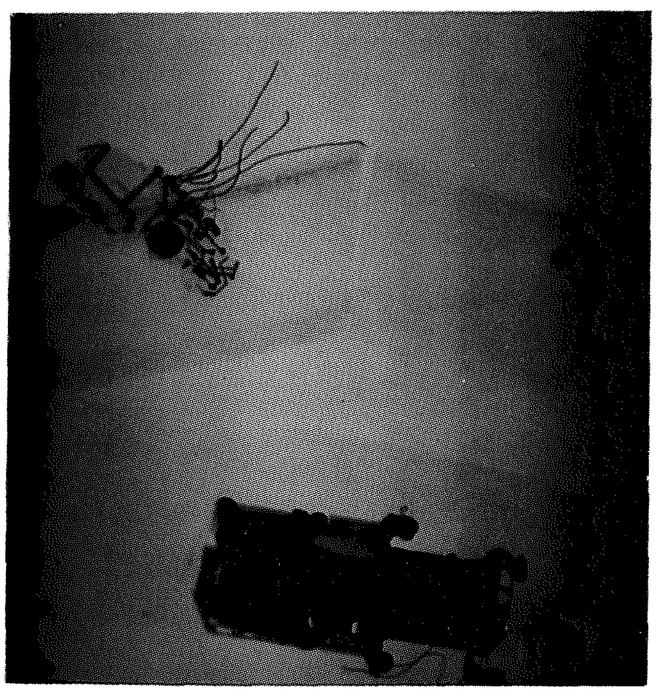

(b) Section View

FIGURE 3: Penetration of Battery Timer and P. C. Board into Dome Material

(a) Top X-Ray View

(b) Section View

FIGURE 4: Penetration of Safe Arm Slide Timer into Dome Material

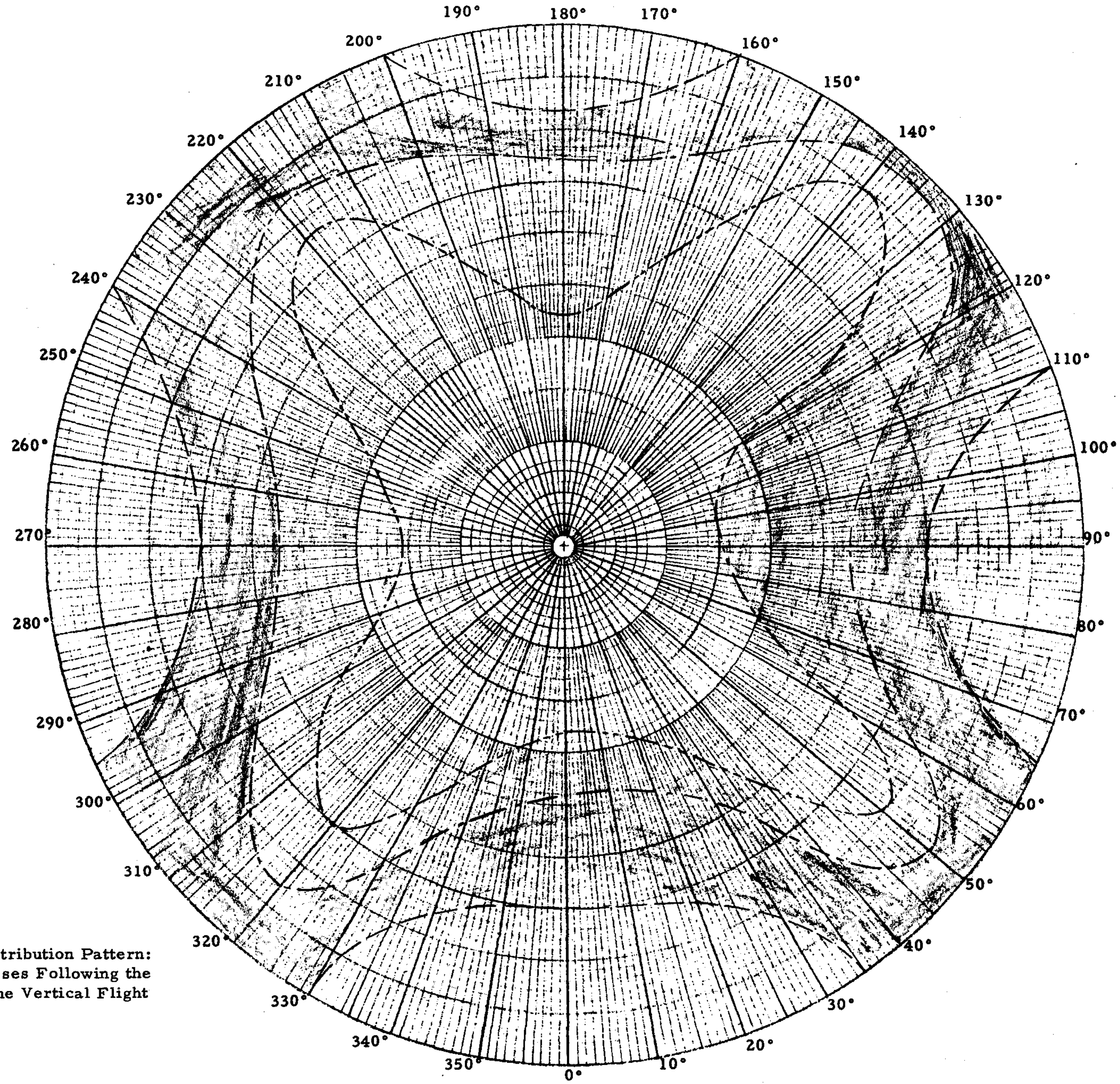

FIGURE 5: Soil Debris Distribution Pattern: Density Decreases Following the Increasing of the Vertical Flight Angle

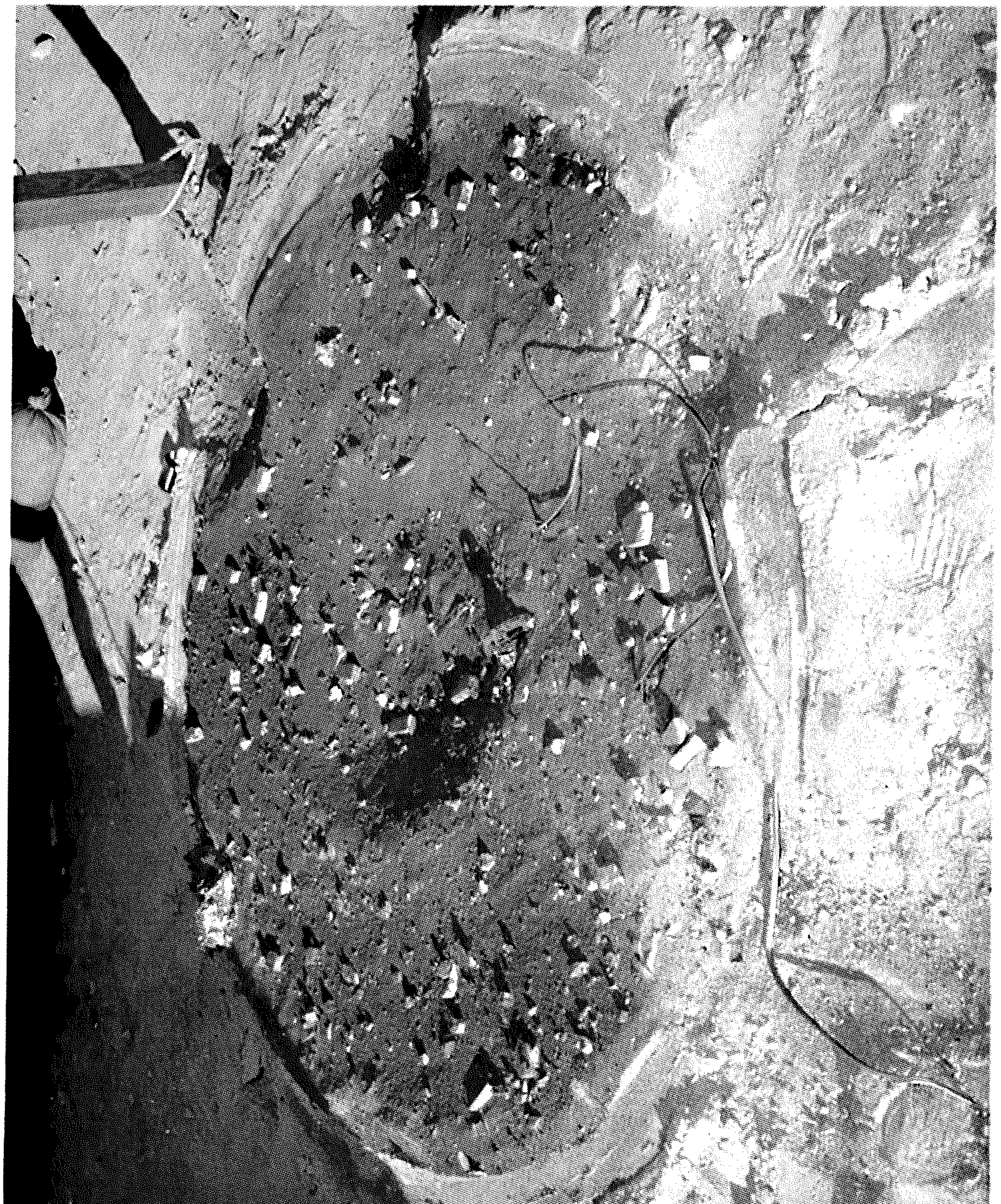

FIGURE 6: Ground After Detonation Under the Dome (One-Eighth Pound Charge)

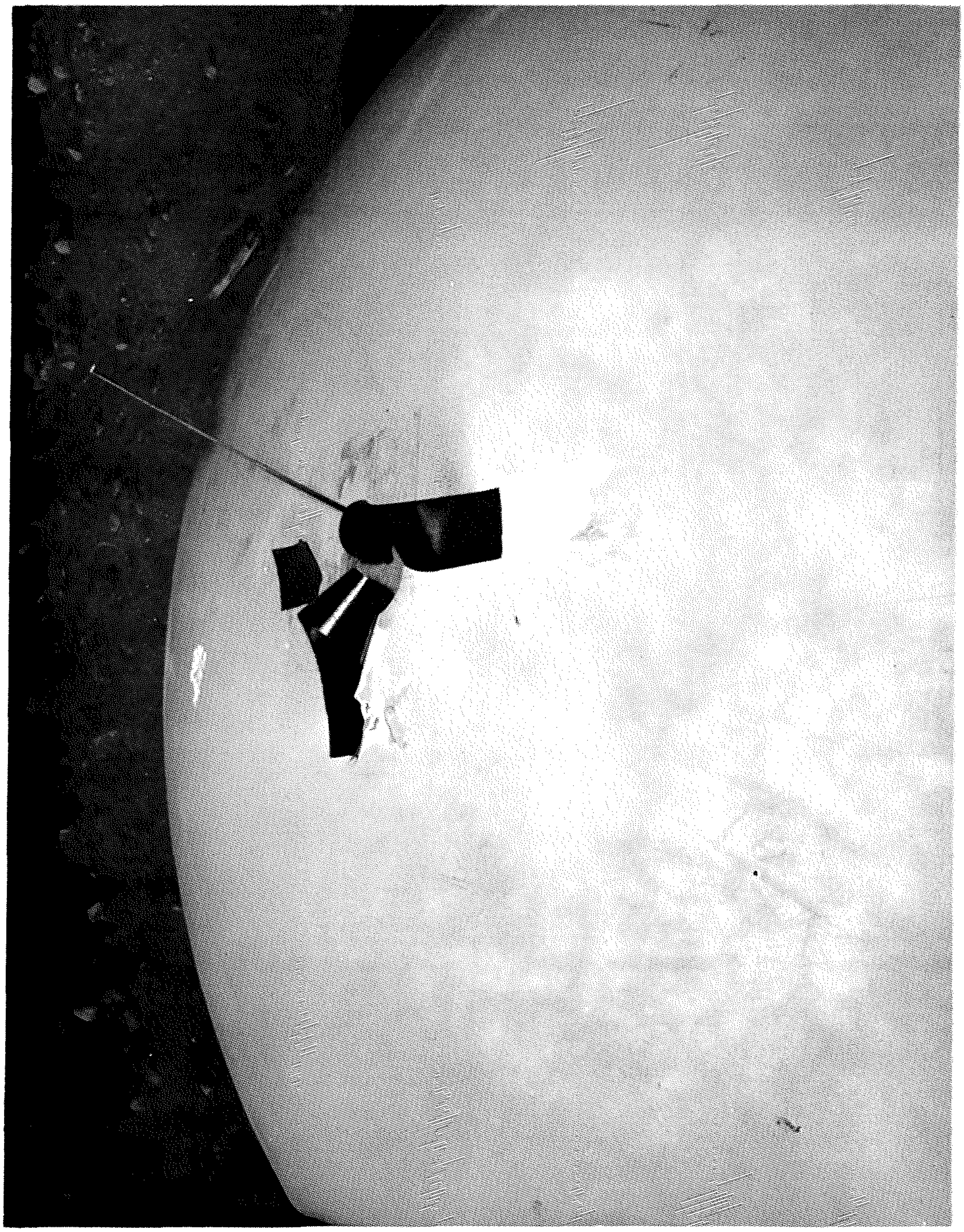

FIGURE 7: Three Spalling Spots on the Surface
of the Dome (One-Eighth Pound Charge)

FIGURE 8: Fragmentation on the Dome (One-Eighth Pound Charge)

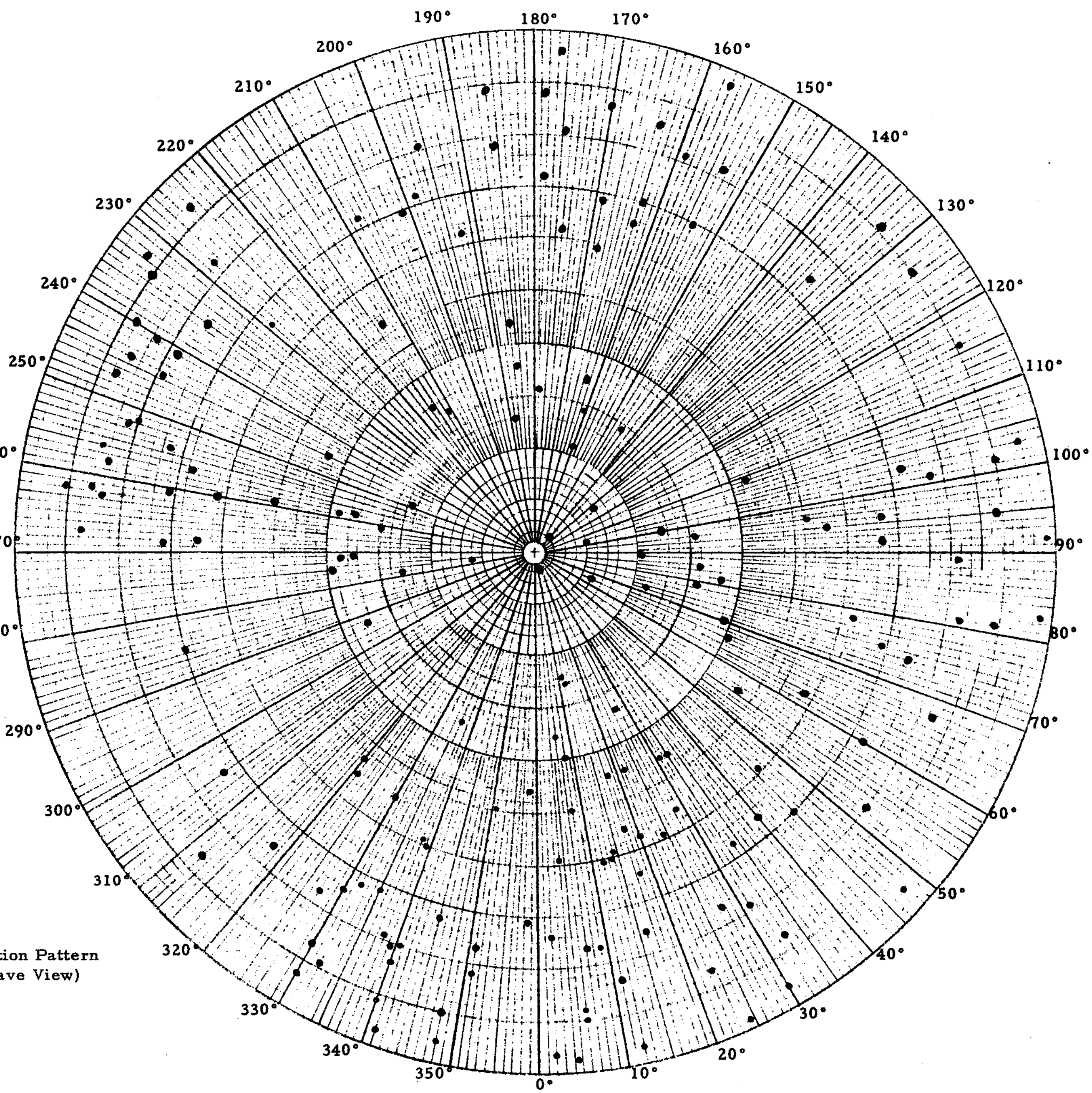

FIGURE 9: Fragment Distribution Pattern on the Dome (Concave View)

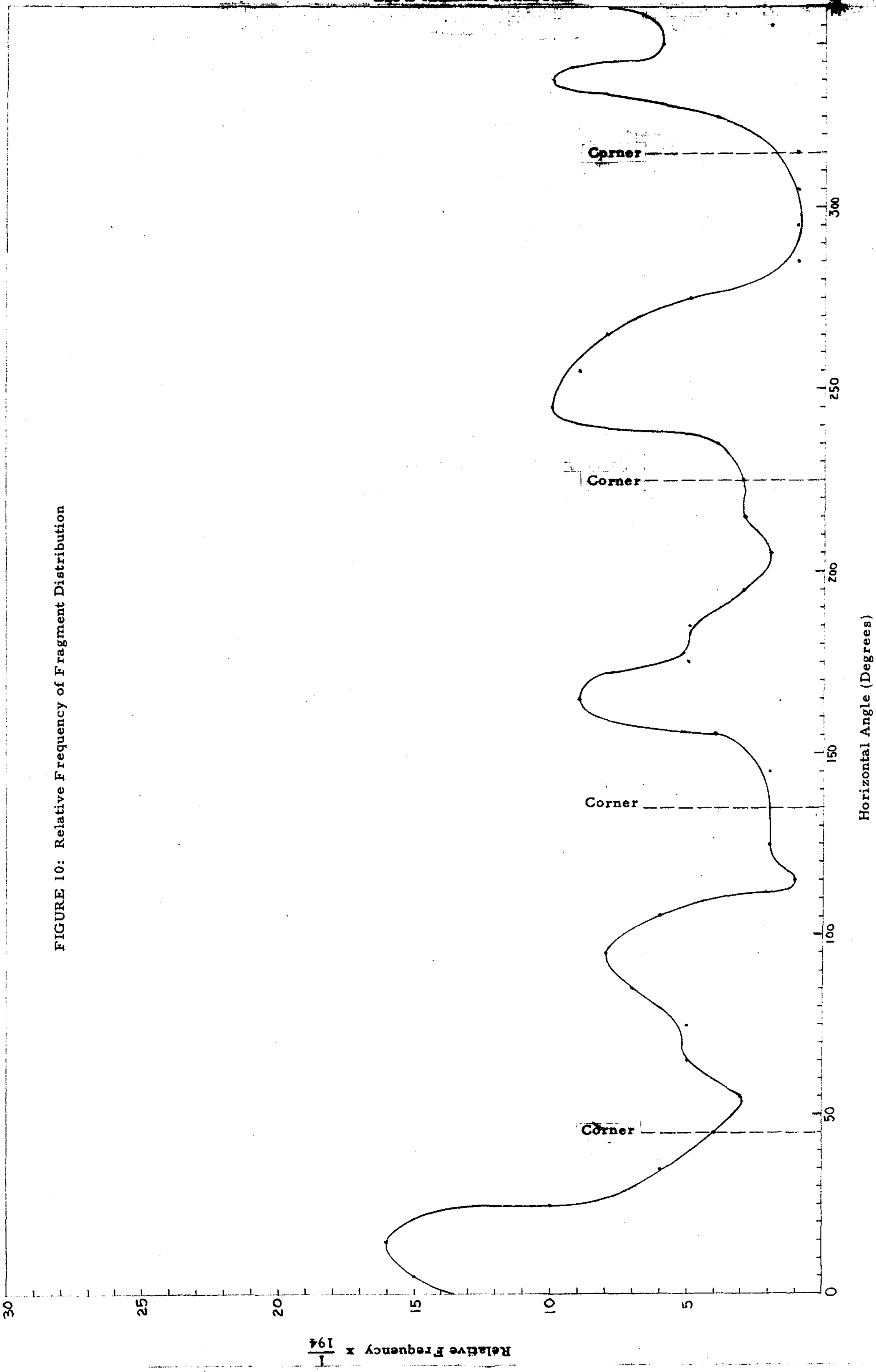

FIGURE 10: Relative Frequency of Fragment Distribution

FIGURE 11: Relative Frequency of Fragment Distribution Versus Initial Vertical Flight Angle

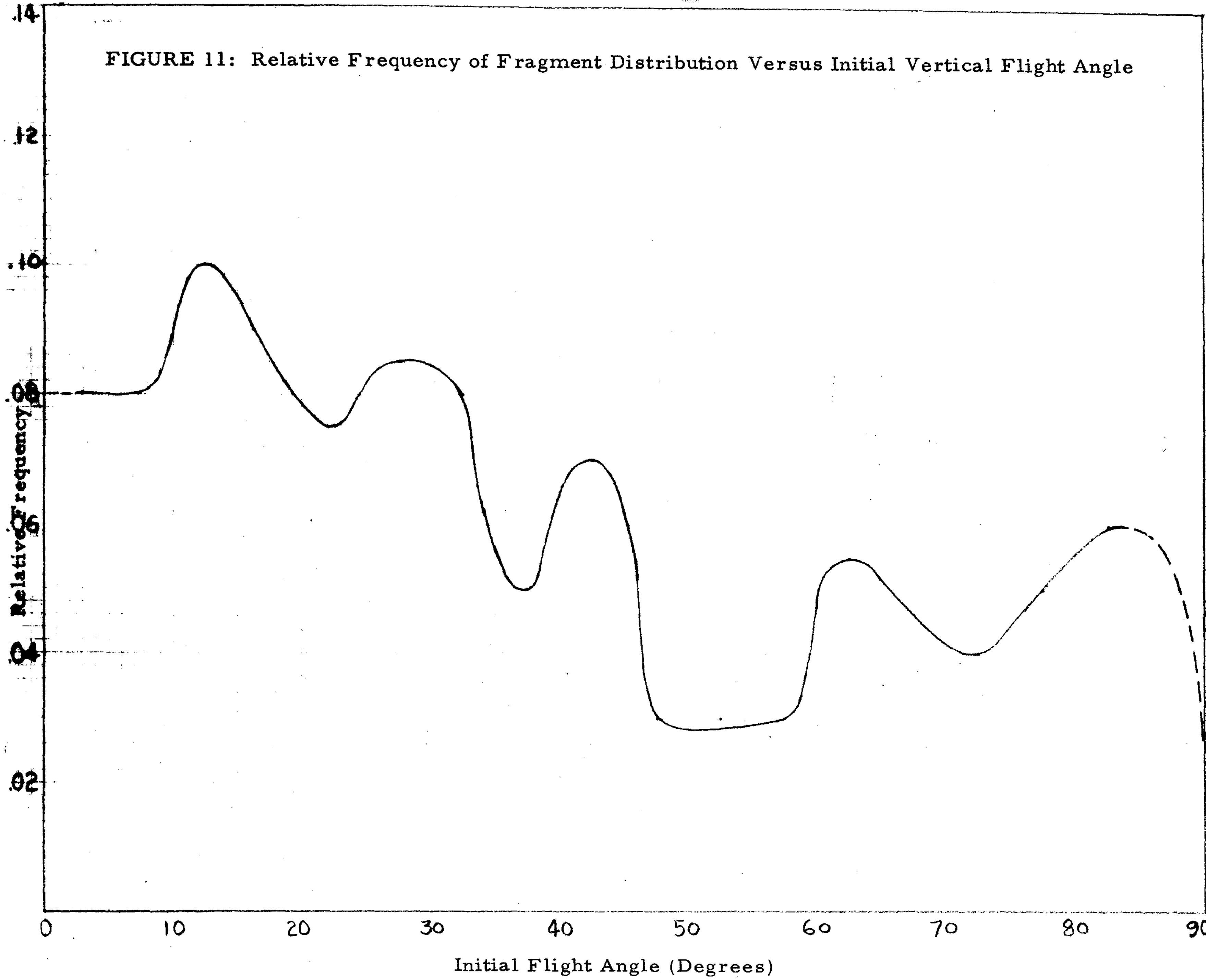

During the cutting and processing of the dome, the information on soil debris was observed. The number and size of debris particles and their penetration in relation to the flight angle are presented in Figure 12. It shows that only a few small-sized particles were accelerated upward. Most debris were flying outward at flight angles of less than 45^o. The horizontal angle, extending from 180^o to 360^o, had an increasing slope with a two-inch mount at mid-point (270^o). This mount was effective in cutting down the amount of debris and fragmentation as is evident in Figures 5, 8 and 9.

IV. CORRELATION AND INTERPRETATION OF DATA

The empirical formula used in this section for predicting the fragment velocity was derived through statistical interpretation of the previous calibration test. This formula is presented as follows:

$$\frac{p}{d} = 66.491 \frac{\left(\frac{mv^2}{2\sigma}\right)^{2/3}}{A} \left(\frac{\rho_t}{\rho_p}\right)^{.64639} \qquad (1)$$

where p, d, m, v, σ, A, ρ_t and ρ_p are defined in Appendix.

By eliminating the possible misinterpreted penetration points, a total of 76 fragments, as tabulated in Table 1, was selected from the collected raw data. These data formed a statistical base to calculate the velocity and the hazard probability. By rearranging Equation (1) the velocity was correlated through this relationship.

$$v = \left\{ \frac{2\sigma}{m} \left[\frac{1}{66.491} \left(\frac{\rho_p}{\rho_t}\right)^{.64639} \cdot \frac{p}{d} A \right]^{1.5} \right\}^{1/2} \qquad (2)$$

The results were presented in the last column of Table 1 and were then plotted versus fragment weight in Figure 13. It shows that the heavier fragments have slower velocity. The soil debris have a lower velocity distribution than that which is indicated in Equation (2) for fragments. Examination of the whole velocity range shows that one data point has a deviated high velocity of 1915 fps (with p/d = 191.667 indicating a bad point). By discarding this point the relative frequency of this velocity spectrum was plotted in Figure 14. It resembles a chi-square distribution in a lower degree of freedom. The cumulative frequency relative to this velocity was then plotted in Figure 15. By scaling down the velocity parameter and using polynomial regression technique, the equation relating cumulative frequency to velocity range is obtained as follows:

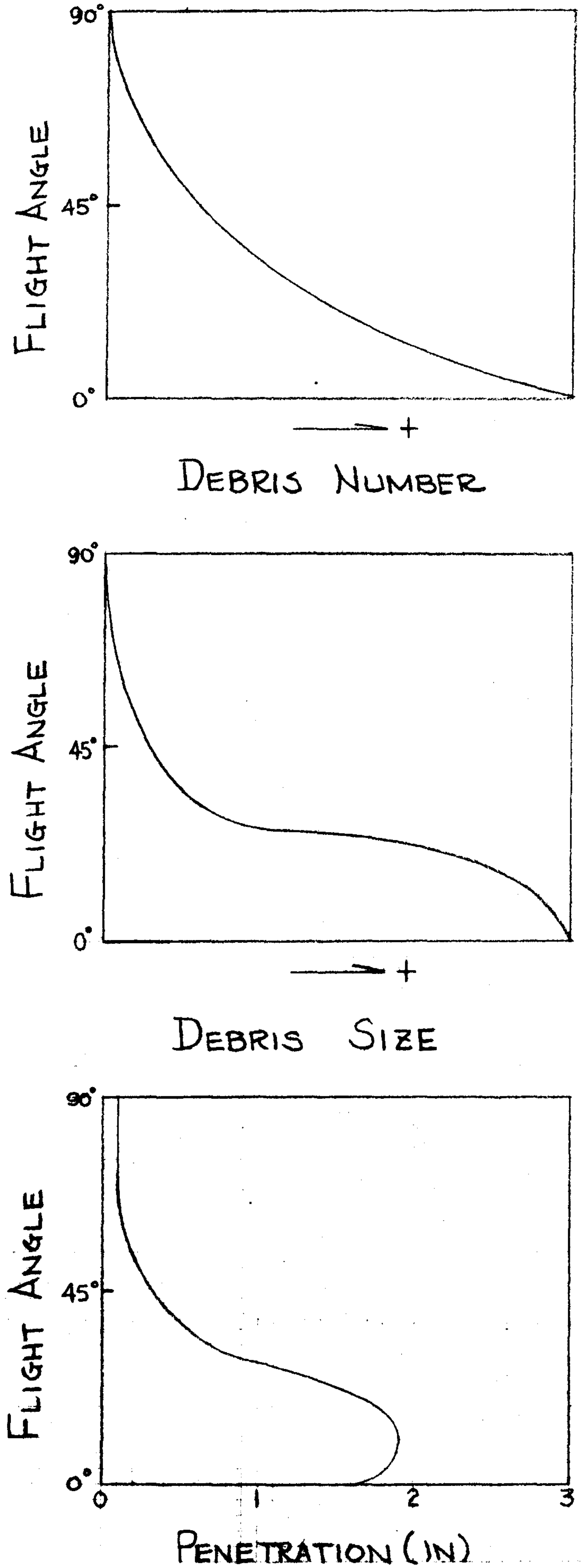

FIGURE 12:

Observed Distribution and Penetration Pattern of Soil Debris Versus Vertical Flight Angle

FRAG. NO.	Θ_H (DEGREES)	Θ_V (DEGREES)	PENET. D (INCHES)	WEIGHT (GRAMS)	LEAST D (INCHES)	AREA (IN^2)	MAT'L DENSITY (LB/FT^3)	MEAN VELOCITY (FT/SEC)
I - 1	11	75	.31	.2	.06	.09375	165	174.9
I - 4	8	60	.52	.3	.125	.0625	165	89.5
I - 9	27.7	44	1.90	3.1	.0469	.125	165	246.2
I - 10	46	41	2.0	2.0	.125	.125	165	160.2
I - 14	336	64.5	.52	2.1	.166	.25	165	77.4
I - 16	27	66	1.875	.2	.08	.03125	165	238.5
I - 25	20	42	2.0	1.2	.218	.11	165	123.8
I - 30	327	23	2.0	3.8	.375	.41	165	124.3
I - 31	330	25	1.55	1.47	.3125	.0976	165	64.5
I - 32	335	28	.625	.6	.18	.132	181	98.5
I - 33	332	27.5	1.52	.55	.05	.02	165	125.1
I - 35	339.2	19	1.3	1.4	.56	.68	165	160.3
I - 36	340.5	20	1.0	.65	.3	.12	165	84.0
I - 38	330	13	2.0	.40	.0313	.05	165	51.0
I - 0	350.7	45	1.75	.11	.06	.028	165	349.0
I - 39	332.	10.8	1.1	.9	.218	.06	181	58.9
I - 40	358.5	29	3.04	11.6	.094	.067	165	90.0
I - 42	16	24.3	2.875	.3	.015	.06	165	1915.0
I - 44	31	21.5	2.0	.6	.063	.2735	165	879.5
I - 48	7	23	.25	.6	.375	.2813	181	50.4
I - 52	320	48.5	.59	.4	.046	.2815	181	567.4
I - 53	48	13.5	3.875	1.2	.28	.0703	181	169.1
I - 54	344	20.	1.38	6.65	.21	3.0	181	497.0
I - D1	4.7	2.	1.1	4.1	.625	.75	181	83.3
I - E1	6.	11.5	2.22	.7	.05	.025	165	199.3
I - E2	340	8.4	1.95	2.4	.30	.12	165	72.2
I - F1	348	4	.24	.21	.1875	.048	165	36.3
I - F2	341	3.4	1.75	3.4	.68	.375	165	71.1
I - E3	348	10	1.75	1.3	.218	.14	165	129.0
I - G1	9	23	.50	2.5	.21	.527	165	101.0
I - E4	300	82	1.6	119.	.969	2.75	165	38.2
II - 1	109	57	1.25	88.3	1.25	2.7313	165	30.5
II - 2	104	85	2.05	2.8	.375	.126	165	67.9
II - 3	127	83	.25	2.4	.25	.4	181	44.5
II - 4	65	84	1.2	1.4	.0625	.0469	165	104.8
II - 5	89	79	2.0	2.6	.375	.28125	165	113.2
II - 7	100	75	1.5	3.6	.1875	.1172	165	67.6
II - 8	79	68	2.11	4.0	.4	.24	165	90.5
II - 10	96	69	1.1	1.0	.094	.25	181	307.0
II - 11	81.4	63.5	2.2	1.0	.2	.06	165	112.6
II - 12	65	59.5	2.15	.5	.25	.0491	165	113.0
II - 13	56	44	.98	.46	.063	.024	181	96.5
II - 16	95.5	43.5	.46	13.8	.625	.3067	165	11.9
II - 17	78.4	37.5	1.9	9.8	.875	.9844	57	65.7
II - 0	10.3	88.5	4.1	32.2	.8125	1.117	490	580.0
II - 20	52.5	20.0	1.438	.15	.04	.004	165	81.2
II - 21	67.5	17.5	2.125	1.1	.25	.1	165	128.3
II - 23	92	33	2.0	5.6	1.15	1.0387	181	90.2
II - 27	116	9	2.875	.2	.047	.018	165	403.7
II - 28	70	61	2.05	.1	.06	.046	165	667.2
II - A9	101.3	22.5	2.0	.15	.018	.02	181	643.8
III - 1	142	88	4.0	13.1	.188	.168	490	647.5
III - 3	144.8	71	2.32	4.13	.375	.1105	165	57.9
III - 6	111.5	69	2.0	1.7	.0313	.04	181	212.4
III - 8	185	56	1.5	17.15	.12	.469	165	122.5
III - 9	215	56.5	.32	.5	.16	.036	181	269.3
III - 10	213	47	2.0	3.6	.4685	.75	165	169.9
III - 16	201.6	31	.56	.3	.156	.078	110	86.9
III - 19	168	41	1.45	33.0	.25	.56	181	57.7
III - 23	163.8	15	2.0	.4	.0313	.044	181	470.9
III - 28	163	64.5	1.84	193.3	1.406	7.5	165	53.7
III - 33	169	32.4	.15	.1	.125	.049	165	50.9
III - 34	186	11	2.18	.2	.0313	.0078	165	217.1
III - 35	185.5	22	1.52	.1	.105	.0938	181	545.0
IV - 2	248	74.7	2.25	.81	.125	.3125	165	628.4
IV - 3	261	70	2.0	15.2	.875	.5	165	38.2
IV - 4	258	65	.437	8.6	.375	.9375	165	49.1
IV - 6	270.5	65.5	2.2	8.9	.395	.1105	165	35.8
IV - 7	271	63	.49	.5	.3125	.2051	165	81.4
IV - 9	293	65	.05	1.9	1.0	1.25	110	11.4
IV - 11	249	49.7	.16	.4	.25	.125	165	32.0
IV - 16	260.5	28.7	3.48	1.1	.125	.0938	165	351.7
IV - 17	268	34.5	2.5	2.0	.7	.3848	165	143.8
IV - 20	205	25.5	1.875	0.9	.3125	.12	165	111.0
IV - 21	218	24.7	2.28	30.4	.1875	.5	165	109.2
II - 30	80.5	75	.1	17.0	2.25	14.99	165	24.1

TABLE 1: Selected Test Data (One-Eighth Pound Charge)

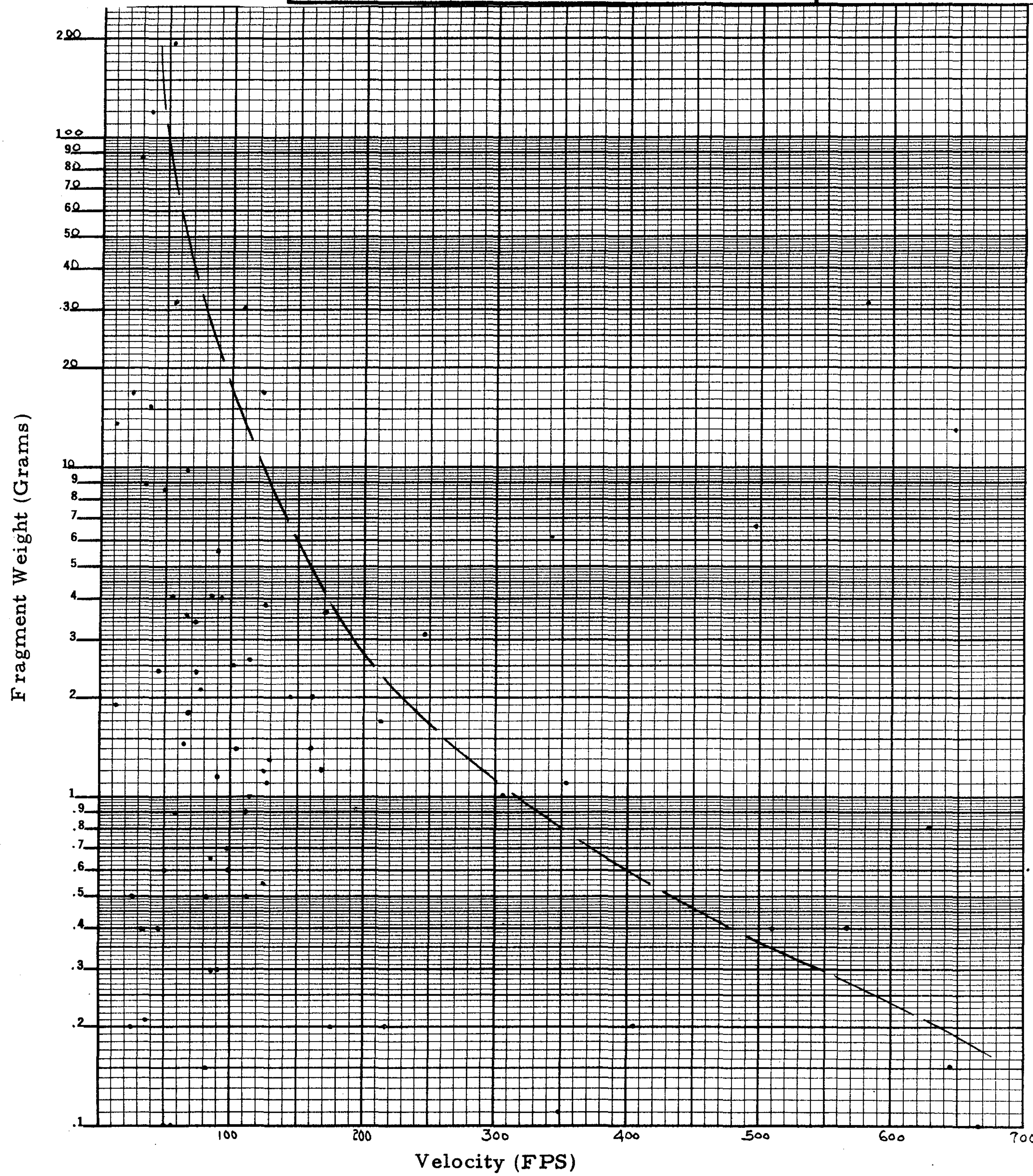

FIGURE 13: Fragment Weight Distribution Versus Initial Velocity

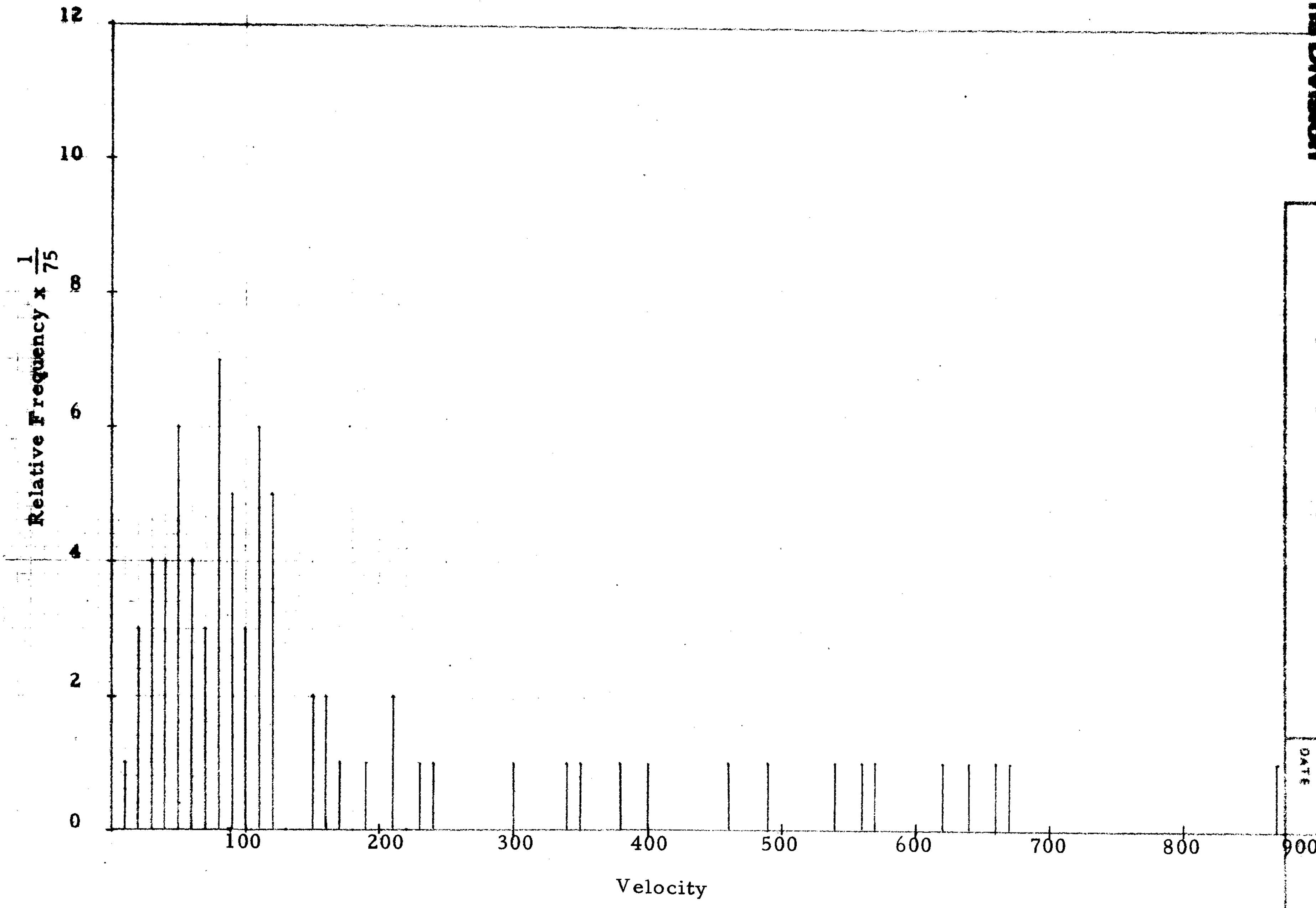

FIGURE 14: Relative Frequency of Fragment Versus Initial Velocity

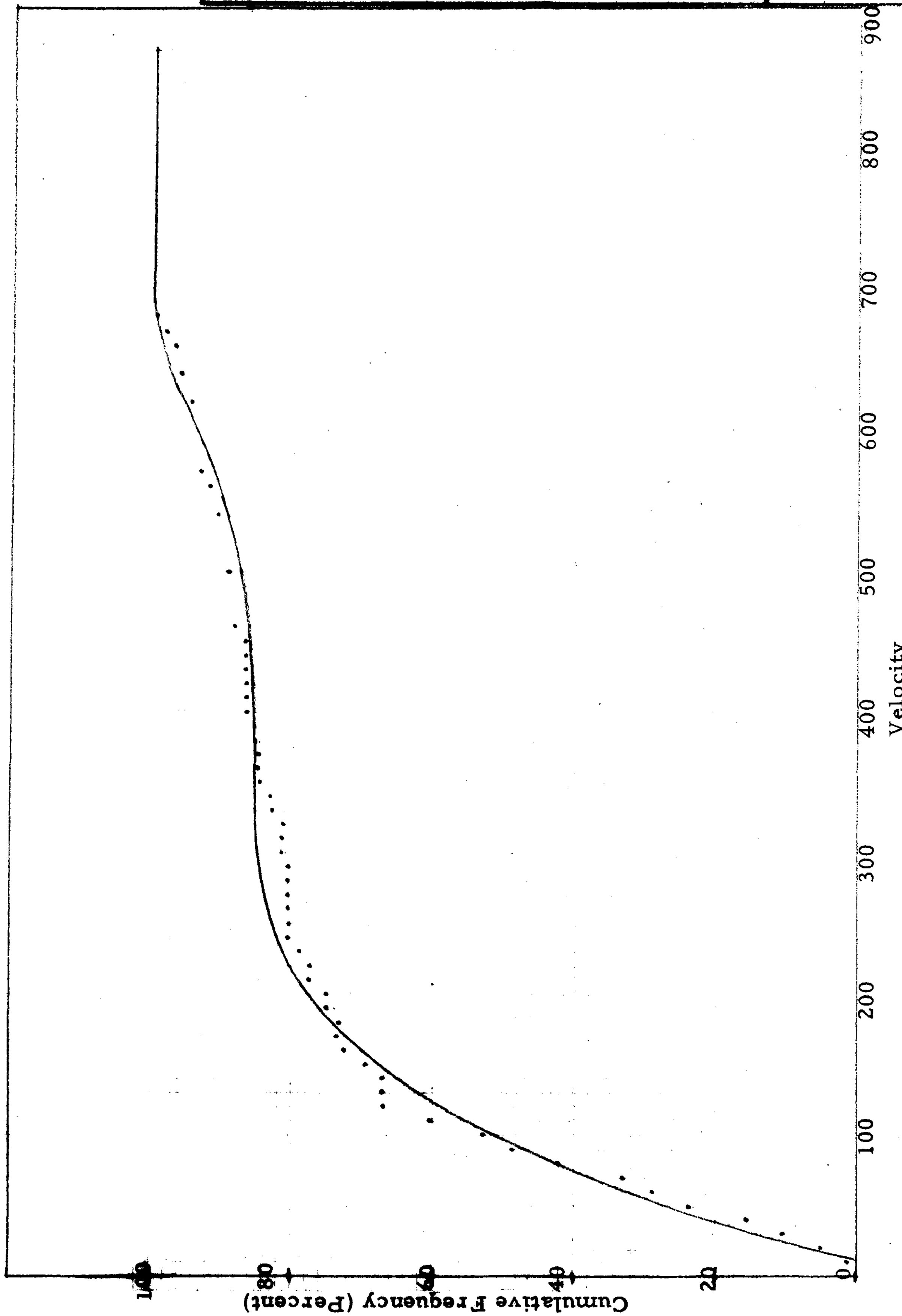

FIGURE 15: Cumulative Frequency of Fragment Versus Initial Velocity

$$F = -11.6558 + 88.9288\, v' - 29.67\, v'^2 + 4.20603\, v'^3 - .207114\, v'^4 \quad (3)$$

where

F = cumulative frequency in percent

$v' = v/100$

Equation (3) is plotted in Figure 15 as a solid line.

V. HAZARD ANALYSIS

A. Hazard to the CSM

The explosive packages are timed to detonate approximately ninety hours after they are deployed on the lunar surface. Under the contingent condition, the CSM may possibly be in lunar orbit during the sequence of explosion. Therefore, there is legitimate concern that fragments and debris from the detonation might possess the potential hazard to the orbiting CSM. From the last column of Table 1 it can be seen that the velocities due to a one-eighth pound charge detonation are lower than 1976 fps (602 m/s) which is the vertical velocity component needed to reach the orbiting CSM. Therefore, no fragment and debris hazard will occur to the CSM as a result of a one-eighth pound charge detonation. Due to the lack of one-fourth pound charge test data the SRI[2] Report on the Active Seismic Experiment are adapted for extrapolation. This report provides the velocity of different sized fragments from the detonation of a one-pound charge as follows:

TABLE 2

Fragment Number	Estimated Fragment Mass (Grams)	Average Velocity (Meters/Sec)	(Ft/Sec)
0	27.5	190	623
1	1.0 ± 0.4	610	2000
2	0.12 ± 0.04	480	1573
3	1.2 ± 0.4	370	1212
4	3.5 ± 0.2	330	1081
5	0.5 ± 0.1	380	1246

By comparing Table 2 with Figure 16 it can be seen that the fragment velocity due to a one-pound or heavier charge is capable of reaching the CSM orbit. Therefore, the conservative results calculated in ATM 1079[1] are valid here. Table 3 repeats this data as follows:

TABLE 3

Charge Weight Pounds	No. of Fragments Based on .001 pound Fragment	Hit Probability Pi
1	2737	1.44×10^{-9}
3	2811	2.609×10^{-9}
6	2814	2.992×10^{-9}

$$P = \sum Pi = 7.041 \times 10^{-9}$$

From the observation of the one-eighth pound charge field test, it can be stated that the velocity and size of soil debris are drastically reduced in the higher flight angles. Therefore, the possibility of some significant debris reaching the CSM orbit is negligible.

B. Hazard to the ALSEP Electronics Central Station (ECS)

Equation (3) provides the cumulative frequency related to velocity range. Since the flight angle θv of each particle is known, the range of velocities (v_1, v_2) that could strike the ECS can be calculated from the Equation (IV-9) of Reference 1:

$$v = \left[\frac{gx^2}{2(x \tan \theta v - y) \cos^2 \theta v} \right]^{1/2} \quad (4)$$

where g is the lunar gravity,

x the horizontal distance, and

y the veritcal coordinate.

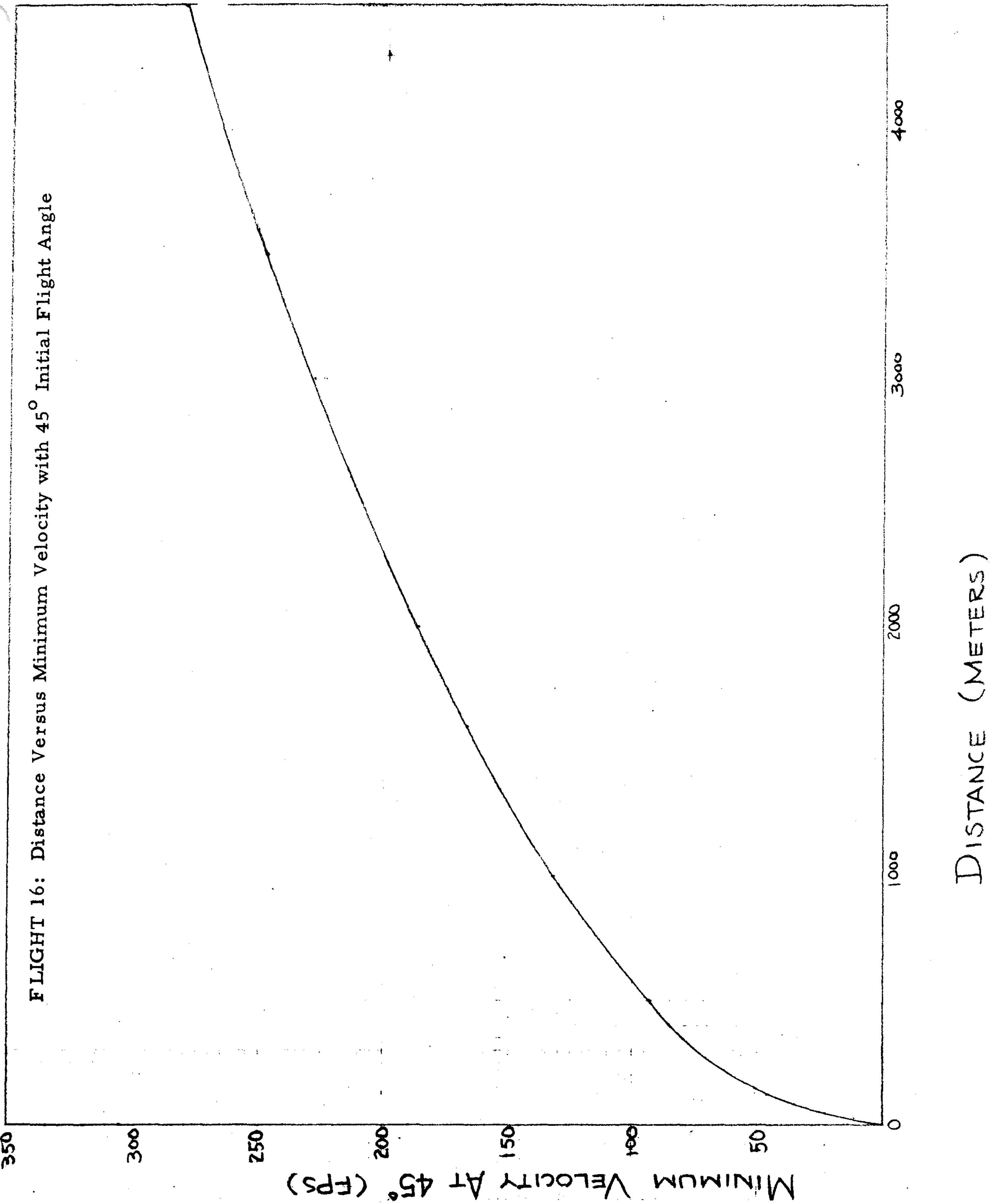

FLIGHT 16: Distance Versus Minimum Velocity with 45° Initial Flight Angle

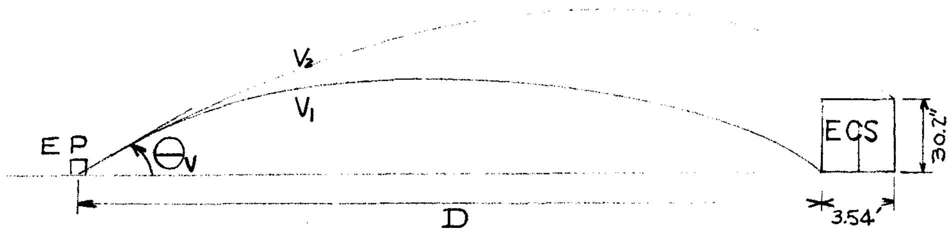

From the above figure it gives:

$$\begin{cases} x = x_1 = D \quad (FT), \quad y = y_1 = 0 \xrightarrow{\text{Equation 4}} v = v_1 \text{ (fps)} \\ x = x_2 = D + 3.54 \text{ (FT)}, \quad y = 30.2/12 \text{ (FT)} \longrightarrow v = v_2 \text{ (fps)} \end{cases}$$

By using Equation (3) the chance of this projectile to be in this velocity range is calculated as follows:

$$P_v = (F_2 - F_1) \qquad (5)$$

where F_2, F_1 are cumulative frequencies by substituting $v_1' = v_1/100$ and $v_2' = v_2/100$ into Equation (3) respectively. The ratio of horizontal angle extended by the largest exposed dimension of the ECS is calculated.

$$P_h = 3.54/2\pi D \qquad (6)$$

By examining through θ_v and θ_h in Table 1, it can be seen that there is no single piece of fragment having the same θ_v and θ_h. The striking probability of each projectile should be an independent event.

$$Pi = P_v \circ P_h \qquad (7)$$

Therefore the probability of a strike occurring to the ECS due to any detonation should be a summation of all those probabilities modified by the weight ratio

$$P = \frac{W}{W_r} \sum_{i=1}^{N} Pi \qquad (8)$$

where W_r is the weight being recovered, W the package weight exclusive of the charge weight, and N is the total number of fragments recovered.

Based on the data collected from the one-eighth pound charge field test and the distance (D = 125 meters) used, the striking probability is calculated to be .000892. Extrapolating from the theoretical computation presented in Reference 1, the hazard to the ECS is tabulated in Table 4:

TABLE 4

Charge Wt. in lbs.	No. of Set	Distance Deployed in Meters	Theoretical Prediction P (%)	Exp. or Extrapolation P (%)
1/8	2	125	.068	.0892
1/4	2	250	.0172	.0225
1/2	1	500	.0045	.0059
1	1	1000	.00148	.00194
3	1	3500	.00019	.000249
6	1	3500	.00029	.00038

$$P = 2\,(.0892 + .0225) + .0059 + .00194 + .000249 + .00038 = .23187\ (\%)$$

The result (P = .23187%) is 31% higher than the theoretical prediction (P = .1769%) which assumed a uniform distribution concept and a higher initial flight velocity.

For the hazard due to soil debris the test has not provided a clear picture to predict the velocity range. The major problem comes from this phenomenon: when the soil projectiles crush into the styrofoam, they continuously fragment into smaller particles as they penetrate their way through the interior of the foam. But based on the observation of penetration depth and distribution pattern, the previous theoretical calculation[1] would provide the striking probability a working base. The volumes of cratering were measured for three field detonations as tabulated in Table 5:

TABLE 5

Charge Wt. in lbs.	Diameter D' (inches)	Depth h (inches)	Volume Equation Used	Volume Measured	Theoretical Volume (FT^3)
1/8	10	1.5	$1/3\ \pi D'^2h$	.0909	.0387
1/4	6	3.25	$2/3\ \pi D'^2h$	.1418	.082
6	31	9.0	$1/3\ \pi D'^2h$	5.2414	3.1

The volume measured is larger than the theoretical volume from Reference 1. Brushing the soil debris around the crater edge into the crater makes it evident that less than 10% of debris from cratering have ejected outward and become flying projectiles. Therefore, the results calculated in Reference 1 can be used here by proportional modification according to the test data. This technique is similar to the full-scale modeling of lunar explosion craters on earth as stated in Reference 3. The results are tabulated in Table 6:

TABLE 6

Charge Wt. in lbs.	No. of Set	Modified Ratio	Probability (ATM 1089) %	Probability Modified %
1/8	2	$\frac{.0909 \times .1}{.0384} = .237$	1.5352	0.364
1/4	2	$\frac{.1418 \times .1}{.082} = .173$	0.8238	0.1425
1/2	1	(.170)	0.4523	0.0769
1	1	(0.170)	0.25189	0.0426
3	1	(0.170)	0.07484	0.0127
6	1	$\frac{5.2415 \times .1}{3.1} = .169$	0.16318	.0276

$$P = 2(.364 + .1425) + .0769 + .0426 + .0127 + .0276 = 1.1728\ (\%)$$

The chance of debris hazard to the ECS is .011728. The combined fragment and debris striking probability to the ECS is .014047 as can be determined from Tables 4 and 6.

VI. CONCLUSIONS AND SUGGESTIONS

Although the test has collected only one set of data from detonation of a one-eighth pound charge under the dome, this data has proved to be effective in justifying and confirming the previous theoretical study. The most important information derived from the test has been the distribution pattern of fragments and soil debris. However, the lack of the one-fourth pound test data obstructs the extrapolation process; again, the SRI(2) data from a one-pound charge is substituted for this purpose.

Based on the results from the one-eighth pound charge detonated under the dome and from the extrapolation technique, it is concluded as follows:

1) The chanee of a hazard to the orbiting CSM is 7.041×10^{-9}.
2) The chance of the Electronics Central Station being impacted is .014047.

The major contribution to the ECS hazard comes from the soil debris (.011728), while the fragments from packages constitute only a minor hazard (.0023187). From the observation, the damage upon impact from the fragments will be more severe than the soil debris.

Some suggestions for reducing the chance of hazard to the ECS have resulted from observation of the distribution pattern. Figures 5, 8, 9 and 10 clearly show that if either of the package's diagonal lines align with the ECS, the chance of hazard can be greatly reduced. The distance at which the ECS is no longer in line of sight is 1630 meters, based on moon curvature and the height of the ECS (30.2 inches). Therefore, at least six of the eight packages which contribute the most chance of hazard will have direct line of sight to the ECS to take the advantage of alignment. The two-inch sloped mount constructed under the dome did cut down some larger sizes of debris traveling in that direction as shown in Figure 8. Thus, any lunar surface protuberance between the explosive charges and the ECS can reduce the amount of particles reaching the ECS.

This report will be updated to include the results of additional field tests including detonation of one more one-eighth pound and two more one-quarter pound explosive packages under domes. These tests are presently scheduled for August 1972.

VII. REFERENCES

1. "LSPE Explosive Package Fragmentation and Cratering Related to Striking Probability Investigation," by G. B. Min, ATM #1079, Bendix Aerospace Systems Division, Ann Arbor, Michigan, December 15, 1971.

2. "Fragment Hazard Associated with the Active Seismic Experiment," by T. J. Ahrens and C. F. Allen, Phase II, Task III, SRI Project FGU6011, May 11, 1967.

3. "Study of Explosives for Lunar Application," NCG Technical Report Number 25, U.S. Army Engineer Nuclear Cratering Group, Livermore, California, February 1971.

APPENDIX

CORRELATION OF CALIBRATION TEST DATA

A1 Introduction

The purpose of this write-up is to evaluate the penetration characteristics of the dome material used in the LSPE field test. The calibration tests on samples provide an empirical formula for predicting the velocity of the fragments generated by the explosive packages. The factors involved in evaluating the penetration are velocity, contact area, mass and density of target, and projectile materials. The Bendix X-ray unit was used for determining the penetration depth. A total of four separate tests were conducted to cover the entire possible velocity range.

A2 Target, Projectile and Set-Up

The target samples were made by Excello Corporation (also the dome vendor) using the same materials with the same layer thickness as the dome, except that one large flat piece was molded. Sufficient material was obtained to make fifty-four 4" x 4" x 11" sized targets.

Three different projectile materials - lead, plastic and copper-coated steel — were used in tests. A wide range of projectile shapes and sizes was adopted for the tests. Shotgun firings provided spherical projectiles in the size range between BB's and 00 shot and in the velocity range from 675 to 1180 feet per second. Lower velocities (265 feet per second) were obtained by the use of a shot peen machine utilizing very small pellets. A BB air gun with small steel balls provided the first layer penetration range.

The set-up for shotgun firing utilized the Ann Arbor Police firing range and a private test set-up with chronograph. The penetration test using the shot peen machine was performed at Bellevue Processing Corporation located in Detroit. The shot peen machine has a fixed velocity of 265 fps and is restricted to small projectile sizes.

A3 Experimental Technique and Data

Several different techniques were used in this calibration. All of the results are tabulated in Tables A1 and A2. The first technique used a thirty-inch barrel, full-choke, twelve-gauge shotgun firing with varied sizes of shotgun shells. Tests 1 and 3 in Table A1 are in this category. The weight of the pellets recovered from the target had a deviation averaging less than one percent from the standard manufacturer's listing, but the deviation of shot velocity from the chart provided by Remington Company may reach a maximum of 20 percent. All the tests which used this technique have resulted in establishing the following:

1) The energy boundary for puncturing the sample,

2) The lower limit velocity in completely penetrating the foam and impacting the fiber base,

3) The velocity which will spall the outer fiber glass layer, and

4) The velocity which will partially penetrate the fiber glass.

However, low penetrations into the first and second layers was not achieved.

The second technique used the shot peen machine in Test 2. The results are tabulated in Table A1 and two penetration patterns are presented in Figure A2. Since the machine owner restricted the projectile sizes and shapes which could be used with the shot peen machine, the tests were suspended after getting four tested samples. Because the machine can precisely control the velocity at a fixed rate of 265 fps, the penetration can be calibrated and predicted in a narrow range only.

Following the investigation of these two techniques, the third technique was developed to solve the problems associated with the above test methods.

Problem 1: Propelling various sizes of projectiles with the proper velocity range.

Problem 2: Accurately measuring the particle velocity just before impact with the target.

Based on previous knowledge and experience, the third technique approached the problems as follows:

Several different projectiles were available for use: A BB air gun, a 5 mm pellet rifle and a 5.5 mm (.22 caliber) pellet rifle. For controlling particle velocities, the air charge intensity for the particle was varied using a 5 mm pump type pellet rifle. Larger and/or heavier particle penetration data were obtained through hand loading the desired size shot in a shotgun.

Accurate particle velocity was measured by setting the plates of a chronograph (Figure A1) immediately adjacent to the target. This Oehler Research Model 20 Digital Chronograph has a 6 mc clock that gives a four-digit read-out with velocities to the nearest .1 ft/sec. The test results using this last technique were tabulated in Table A2. Some clear penetration patterns were shown in Figures A3 and A4. The results from this technique provide most of the meaningful interpretation in the whole calibration process.

A4 Correlation of Penetration Data

The plot of penetration (p) over least dimension (d) versus velocity of the test data (Figure A5) shows a strong random characteristic. It involves many physical properties entering into the penetration problem. Thus it is a great advantage to express empirical expressions in non-dimensional form among those quantities.

$\frac{p}{d}$ penetration ratio

$T = \frac{\rho_p}{\rho_t}$ density ratio (ρ_p = projectile density; ρ_t = target density)

$B = \left(\frac{mv^2}{2\sigma}\right)^{2/3} \Big/ A$ energy ratio (m = mass; v = velocity; A = contact area; σ = compressive stress of target)

It is likely now that the penetration may be expressed as a function of the above paramenter, i.e., $\frac{p}{d} = F\,(T,\ B)$

Those expressions which are dimensionally correct are mostly in the form of a simple power law: $\frac{p}{d} = kBT^j$ where k is a constant.

This can be transformed to the following form by taking logarithm of both sides:

$$\ln\left[\left(\frac{p}{d}\right)/B\right] = \ln k + j \ln T$$

or

$$Y = \bar{A} + CX$$

where

$$Y = \ln\left[\left(\frac{p}{d}\right)/B\right]; \quad \bar{A} = \ln k; \quad C = j; \quad X = \ln T$$

This equation has the linear form, and the least square analysis discussed in any textbook would apply here to find $\bar{A}$ and C.

A linear regression computer program was written to handle the mass of data in various combinations. The different material property of each layer was incorporated in the computer program as follows:

$$\begin{cases} \rho_t = 3 \ (\#/FT^3) \\ \sigma = 80 \times 144 \ (\#/FT^2) \end{cases} \qquad p \leq 2.0$$

$$\begin{cases} \rho_t = (3 + 8) \left[\frac{(p - 2.0)}{2} + 1.0\right]/4 \ (\#/FT^3) \\ \sigma = (80 + 300) \times 144 \left[\frac{(p - 2.0)}{2} + 1.0\right]/4 \ (\#/FT^2) \end{cases} \qquad 2 < p \leq 4$$

$$\begin{cases} \rho_t = 918 \ (\#/FT^3) \\ \sigma = 5390 \times 144 \ (\#/FT^2) \end{cases} \qquad p > 4.0$$

The result and its error estimation are presented as follows:

$$\frac{p}{d} = 66.491 \frac{\left(\frac{mv^2}{2\sigma}\right)^{2/3}}{A} \left(\frac{\rho_t}{\rho_p}\right)^{.64639}$$

with

Standard error of estimate = .20559

Standard error of C = .05043

Correlation coefficient = .95054

This correlation formula will be used in interpretating the data collected from the field tests of the dome cover.

TABLE A1: TEST DATA AND RESULTS

TEST 1: SHOT GUN SHELL

No.	Shot Type	Size No.	Diameter (in.)	Weight # / Mass (# - sec / ft)	Shot Distance (Yards)	Velocity From Chart (FPS)	Energy Calculated (Ft - #)	Penetration Depth (inch)	Penetration Description
1	Shot	BB	.18	$\frac{.00125}{.3882x10^{-4}}$	12.5	1165	26.34	≥ 4	Bounce and embedded on fiber base
2	Buck	1	.30	$\frac{.005714}{1.775x10^{-4}}$	12.5	1030	94.16	> 4	Cluster type-pentrate half way thru fiber
3	Buck	1	.30	$\frac{.005714}{1.775x10^{-4}}$	25.0	905	72.69	≥ 4	Rest on fiber base
4	Buck	00	.33	$\frac{.007692}{2.3889x10^{-4}}$	12.5	1180	156.22	> 4	Penetrate into fiber
5	Buck	00	.33	$\frac{.007692}{2.3889x10^{-4}}$	25.0	1100	144.53	> 4	Crater fiber base

TEST 2: SHOT PEEN MACHINE

No.	Duration	Size No.	Diameter (inch)	Weight (#) / #-sec / Ft	Velocity (FPS)	Energy (#-Ft)	Penetration Mean Depth (in)	Penetration Description
1		230	.0197	$\frac{1 \times 10^{-6}}{2.59x10^{-9}}$	265	$.182 \times 10^{-3}$	.9468	Concentrate penetration along center line
2		550	.0469	$\frac{13.504 \times 10^{-6}}{3.495x10^{-8}}$	265	$2.454x10^{-3}$	.7484	Uniformly distributed pellets on surface
3	ON-OFF	170	.0138	$\frac{.344x10^{-6}}{.8903x10^{-7}}$	265	$.0625x10^{-3}$	.3659	Uniformly distributed pellets on surface
4	2 seconds	170	.0138	$\frac{.344x10^{-6}}{.8903x10^{-9}}$	265	$.0625 \times 10^{-3}$		Cut half of 1st layer

TEST 3: SHOT GUN SHELL

No.	Shot Type	Size No.	Diameter (in.)	Weight # / Mass (# - sec / ft)	Velocity Shot Distance (Yards)	Velocity From Chart (FPS)	Enegery Calculated (Ft - #)	Penetration Depth (inch)	Penetration Description
1	Buck	00	.33	$\frac{.007692}{2.3889x10^{-4}}$	60	930	103.31	4	Rest on fiber base
2	Buck	0	.32	$\frac{.000897}{2.1418x10^{-4}}$	60	915	89.66	4	Rest on fiber base
3	Buck	1	.30	$\frac{.0057143}{1.775x10^{-4}}$	60	675	40.44	4	Cluster type-fiber & foam separated
4	Buck	4	.24	$\frac{.0029412}{.9134x10^{-4}}$	60	860	33.78	4	Rest on fiber base trapped in 2nd layer of foam close to fiber
5	Shot	BB	.18	$\frac{.00125}{.3882x10^{-4}}$	60	800	12.42	3.88	Trapped in 2nd layer of foam close to fiber
6	Buck	0	.32	$\frac{.000897}{2.148x10^{-4}}$	40	1005	108.16	4	Penetrate and rest on fiber base
7	Buck	1	.30	$\frac{.0057143}{1.775x10^{-4}}$	40	790	55.39	4	Rest on fiber base
8	Shot	BB	.18	$\frac{.00125}{.3882x10^{-4}}$	40	915	16.27	3.92	Embedded between foam and fiber
9	Buck	4	.24	$\frac{.0029412}{.9134x10^{-4}}$	30	1020	47.52	4	Rest on fiber base
10	Shot	BB	.18	$\frac{.00125}{.3882x10^{-4}}$	30	993	19.14	3.98	Trapped in 2nd layer of foam
11	Shot	BB	.18	$\frac{.00125}{.3882 \times 10^{-4}}$	20	1086	22.87	4	Embedded between foam & fiber

TEST SHOT NO	GUN TYPE	SHOT PROPELLANT	PARTICLE TYPE & SHAPE CHAR.	PARTICLE WT. (GRAMS)	PARTICLE MASS (LBS-SEC²/FT)	VELOCITY BEFORE IMPACT (FPS)	PARTICLE DIAMETER (IN)	ENERGY (FT-LBS)	PENETRATION DEPTH (IN)
1	SHERIDAN	AIR (3 PUMPS)	5MM (LEAD)	1.007	.57454 $\times 10^{-5}$	411	.195	.9705	3.6
2	"	AIR (4 PUMPS)	"	1.007	.57454 $\times 10^{-5}$	472	.195	1.280	3.9
3	"	AIR (5 PUMPS)	"	1.007	.57454 $\times 10^{-5}$	515	.195	1.5238	3.91
4	"	AIR (6 PUMPS)	"	1.007	.57454 $\times 10^{-5}$	553	.195	1.757	3.92
5	"	AIR (7 PUMPS)	"	1.007	.57454 $\times 10^{-5}$	583	.195	1.9528	3.93
6	"	AIR (8 PUMPS)	"	1.007	.57454 $\times 10^{-5}$	614	.195	2.166	3.94
7	"	AIR (9 PUMPS)	"	1.007	.57454 $\times 10^{-5}$	635	.195	2.317	3.96
8	38 SPEC 6"	BULL (1.5 gr)	ELONGATED BALL (LEAD)	5.64	3.21787 $\times 10^{-5}$	403	.36	5.226	3.99
9	"		"	5.64	3.21787 $\times 10^{-5}$	368	.36	4.358	3.96
10	"	"	"	5.64	3.21787 $\times 10^{-5}$	291	.36	2.725	3.9
11	"	"	"	5.64	3.21787 $\times 10^{-5}$	352	.36	3.987	3.9
12	38 SPEC (S&W 14-3)	BULLSEYE (1.0 gr)	WAD CUTTER (LEAD)	9.469	5.40249 $\times 10^{-5}$	318	.357	5.4632	4.0
13	"	"	"	9.469	5.40249 $\times 10^{-5}$	246	.357	1.329	3.75
14	"	"	"	9.469	5.40249 $\times 10^{-5}$	278	.357	4.175	3.85
15	"	"	"	9.469	5.40249 $\times 10^{-5}$	322	.357	5.602	4.00
16	"	BULLSEYE (0.5 gr)	PLASTIC CYLINDER	0.959	0.54715 $\times 10^{-5}$	636	.357	2.2132	2.50
17	"	"	"	0.959	0.54715 $\times 10^{-5}$	554	.357	1.679	2.30
18	"	NONE	"	0.959	0.54715 $\times 10^{-5}$	445	.357	1.083	2.40
19	"	"	"	0.959	0.54715 $\times 10^{-5}$	415	.357	.9423	2.005
20	BENJAMIN	AIR (3 PUMPS)	.22 CAL (LEAD)	1.07	0.61048 $\times 10^{-5}$	299	.22	.5458	2.35
21	"	AIR (4 PUMPS)	"	1.07	0.61048 $\times 10^{-5}$	344	.22	.7224	3.00
22	"	AIR (5 PUMPS)	"	1.07	0.61048 $\times 10^{-5}$	429	.22	1.1235	3.45
23	"	AIR (6 PUMPS)	"	1.07	0.61048 $\times 10^{-5}$	480	.22	1.4066	3.90
24	"	AIR (7 PUMPS)	"	1.07	0.61048 $\times 10^{-5}$	518	.22	1.6381	3.95
25	"	AIR (8 PUMPS)	"	1.07	0.61048 $\times 10^{-5}$	544	.22	1.8066	4.0
26	"	AIR (9 PUMPS)	"	1.07	0.61048 $\times 10^{-5}$	562	.22	1.9282	4.0
27	"	AIR (10 PUMPS)	"	1.07	0.61048 $\times 10^{-5}$	544	.22	1.8066	4.0
28	B B GUN	AIR	COPPER COATED STEEL BALL	0.342	0.19513 $\times 10^{-5}$	277	.172	.1497	1.9
29	"	AIR	"	0.342	0.19513 $\times 10^{-5}$	272	.172	.1444	1.96
30	"	AIR	"	0.342	0.19513 $\times 10^{-5}$	214	.172	.0894	1.85
31	"	AIR	"	0.342	0.19513 $\times 10^{-5}$	225	.172	.0988	2.0

CHRONOGRAPH INFORMATION:
OEHLER RESEARCH MODEL 20 DIGITAL CHRONOGRAPH

TABLE A2: Calibration Test Using Chronograph Set-Up

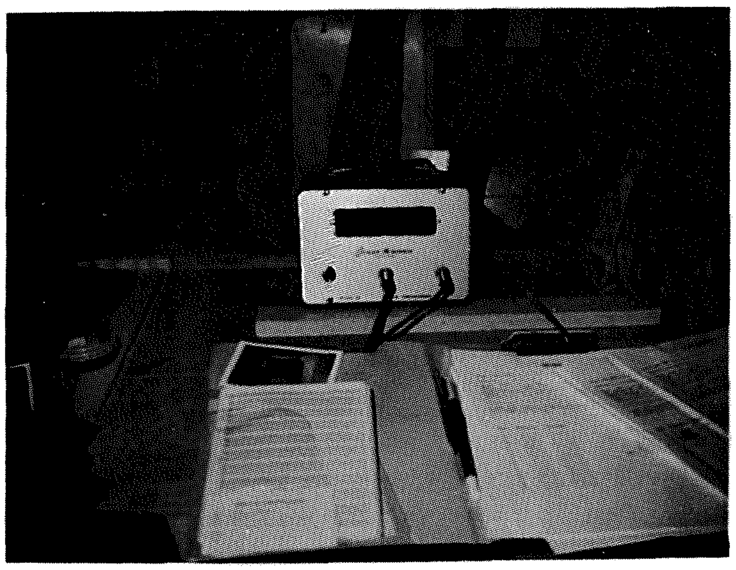

FIGURE A1: Chronograph Set-Up

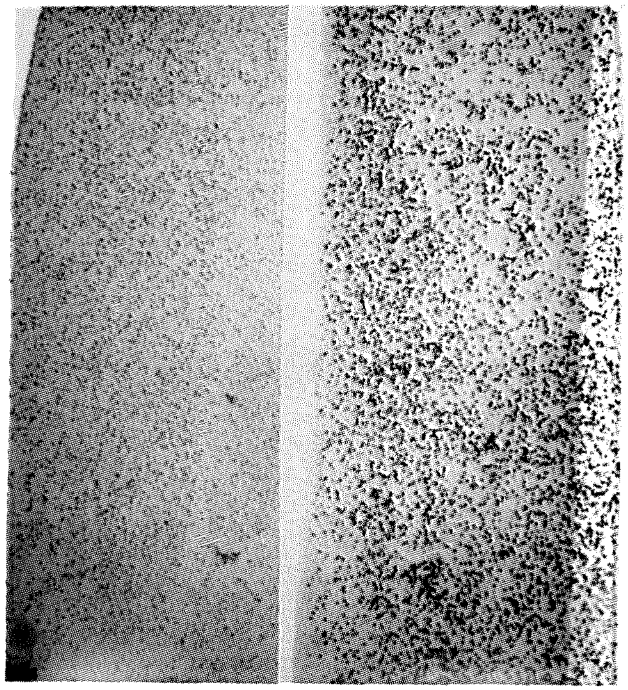

(a) Top View

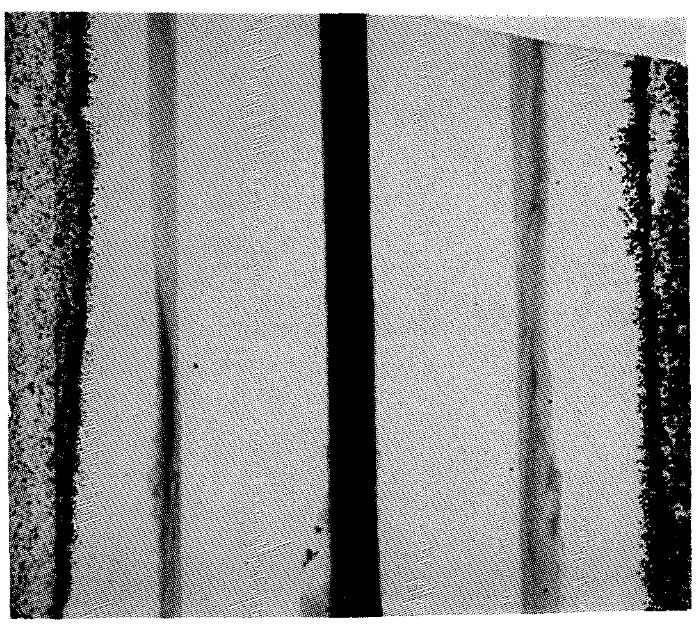

(b) Side View

FIGURE A2: Test 2: Penetration from Shot Peen Machine

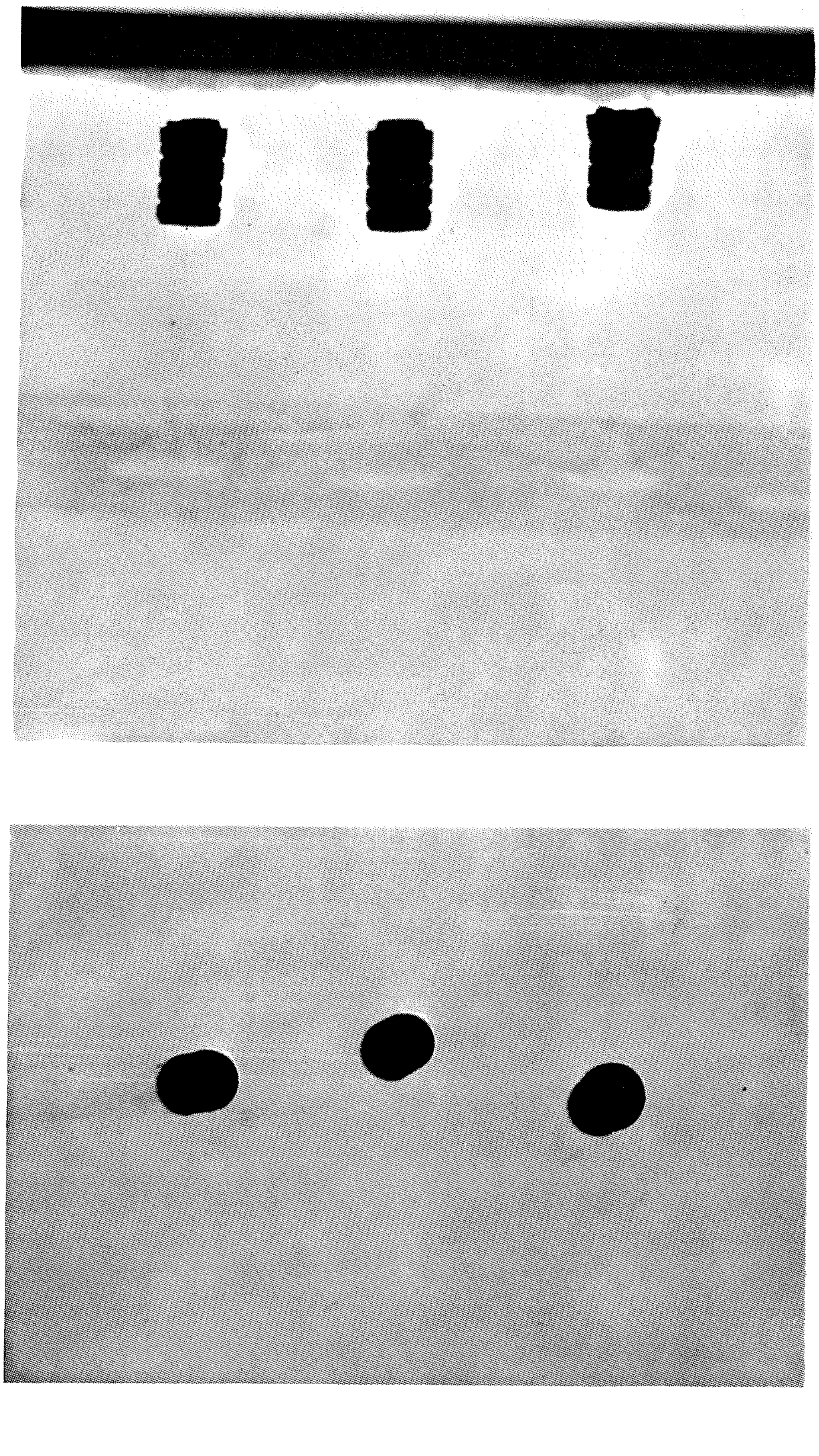

(b) Side View

(a) Top View

FIGURE A3: Test 4 (Shots #12, 13 & 14): Penetration from Wad Cutter Lead Bullet

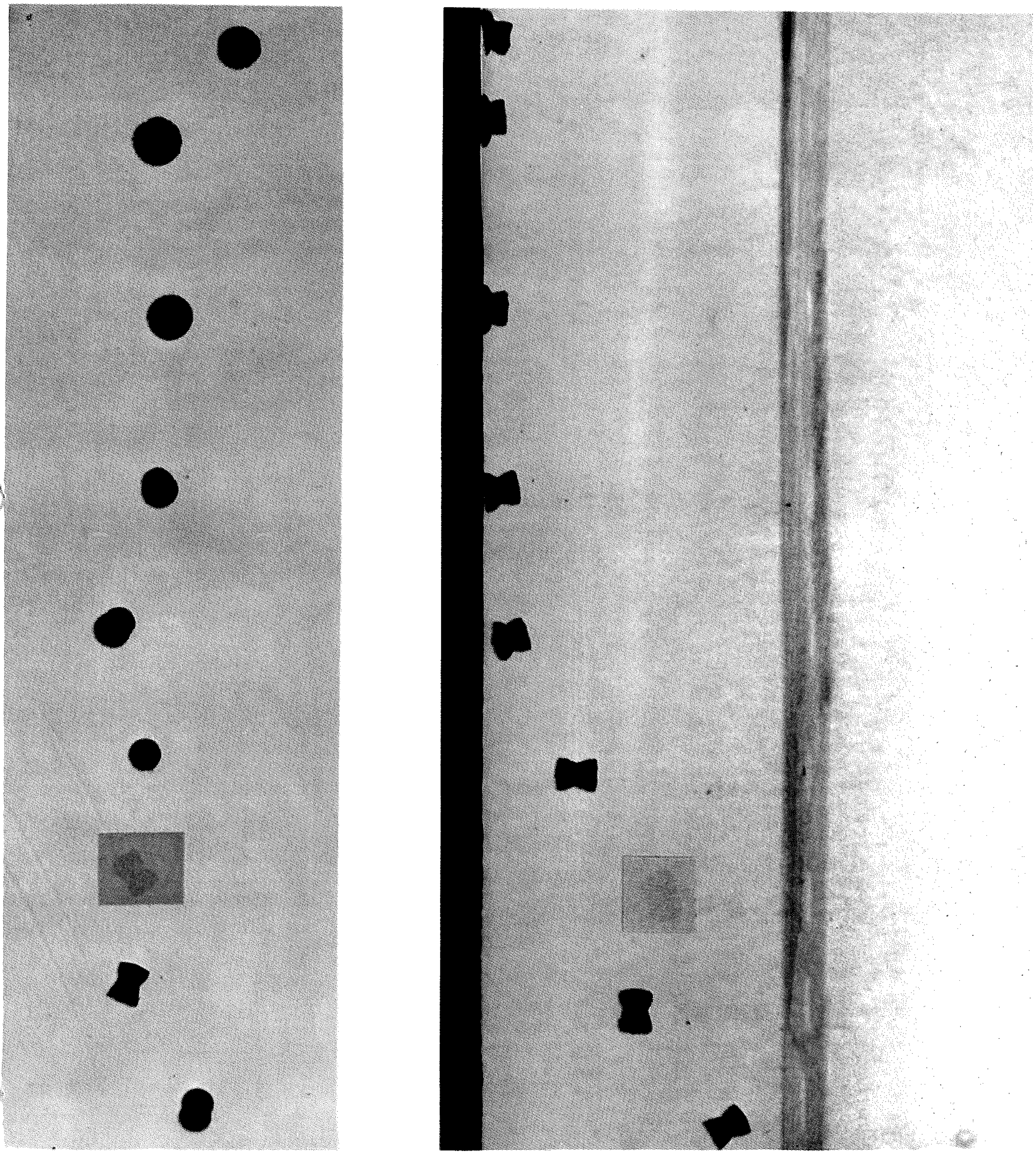

(a) Top View (b) Side View

FIGURE A4: Test 4 (Shot No. 20 ~ 27): Penetration from .22 Cal. Lead Bullet

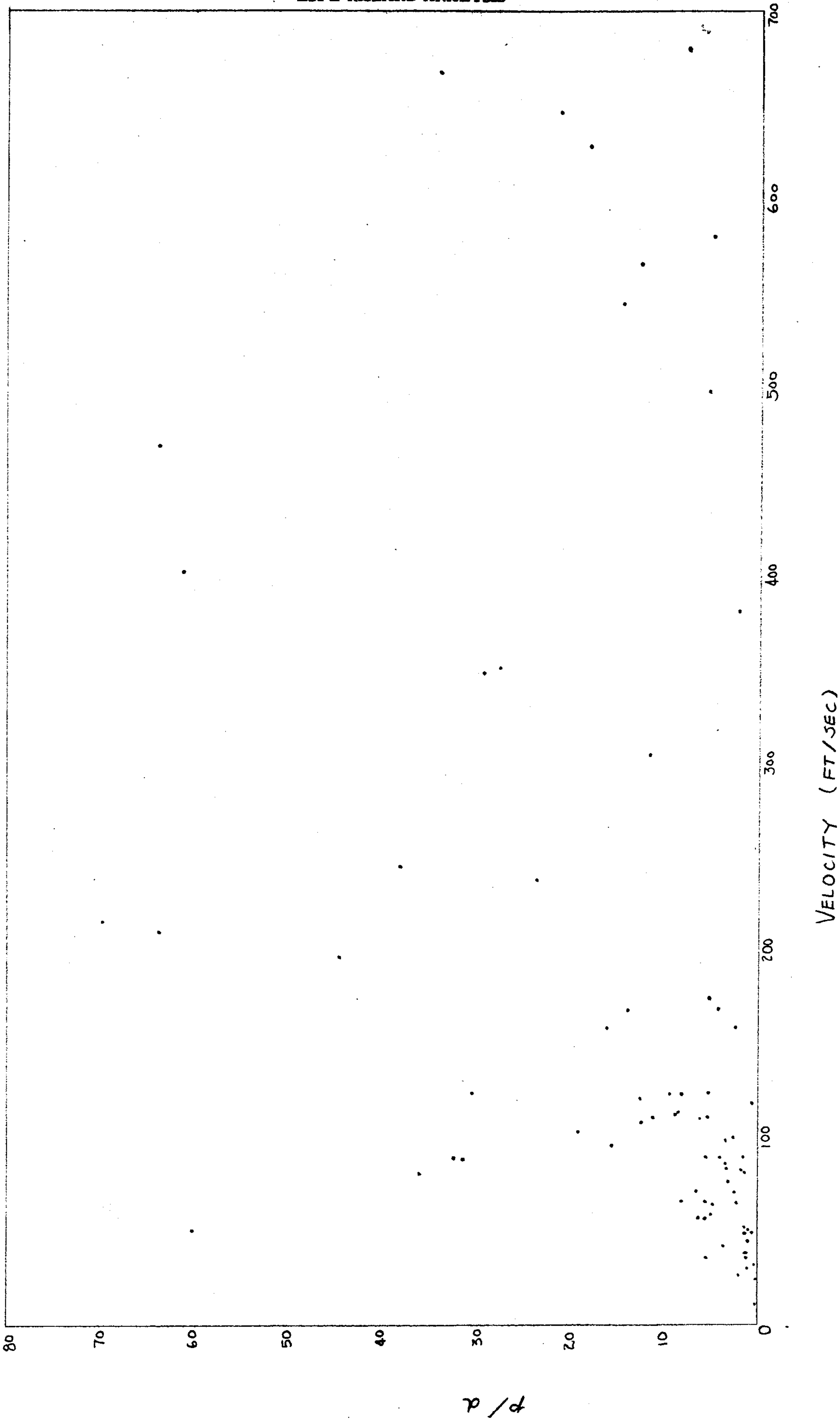

FIGURE A5: Ratio of Penetration Over Least Dimension Versus Velocity